TEMPERATURE DEPENDENT MECHANICAL PROPERTY TESTING OF NITRATE THERMAL STORAGE SALTS

Brian D. Iverson, Scott T. Broome, and Nathan P. Siegel

Concentrating Solar Technologies, Sandia National Laboratories, P.O. Box 5800, Albuquerque, NM, 87185-1127, USA

(505) 844-0480, bdivers@sandia.gov

Abstract

As concentrating solar power applications look to increase operating temperature, salt compounds have received increased attention for use as a heat transfer fluid. However, with the potential of salt freeze events occurring at temperatures above ambient, freeze-recovery remains a concern for industry and financiers alike. Accurate prediction of salt behavior in the solid-phase is necessary for understanding recovery from a freeze event. Mechanical properties for three representative salts (that span a range of melting temperatures) have been obtained as a function of temperature. These properties include compressive strength, tensile strength, Young's modulus and Poisson's ratio. Temperature was not observed to have a significant effect on tensile strength using an indirect tensile test (Brazilian test). Peak stress and Young's modulus (both from unconfined compressive strength testing) were shown to decrease with increasing temperature, whereas Poisson's ratio increased with increasing temperature.

Keywords: salt, mechanical property, solid-phase

1. Introduction

Interest in raising the operating temperature of concentrating solar technologies and the incorporation of thermal storage has motivated studies on the implementation of molten salt as the system working fluid. Recently, salt has been considered for use in trough-based solar collectors and has been shown to offer a reduction in levelized cost of energy as well as increasing availability [1]. Concerns regarding the use of molten salt in troughs are often related to issues with salt solidification and recovery from freeze events. Differences among salts used for heat transfer and storage are typically designated by a comparison of thermal properties and cost. However, the potential for a freeze event necessitates an understanding of salt mechanical properties in the solid phase in order to characterize and mitigate possible detrimental effects during freeze event recovery. This includes stress imparted by the expanding salt.

Initial modeling efforts of tube stress during freeze event recovery have been reported [2]. However, reliable material property data is an integral part to model validation. Previous modeling efforts have assumed mechanical properties similar to published data on common salts. Here, we present data for measured mechanical properties of three common salts used for heat transfer and storage. Samples of solar salt, HITEC salt (Coastal Chemical Co.) and a low melting point quaternary (developed at Sandia National Laboratories) salt were cast for characterization tests to determine unconfined compressive strength, indirect tensile strength, Young's modulus, and Poisson's ratio. Experiments were conducted at multiple temperatures below the melting point to determine temperature dependence in the solid phase. Temperature dependent coefficient of thermal expansion data is anticipated as an extension to this work and data collection is currently underway.

2. Approach

In an effort to span the typical range of melting point possibilities of thermal storage salts, three representative salts were selected for property testing: solar salt (60 wt% $NaNO_3$, 40 wt% KNO_3)[3, 4], HITEC salt [5], and a low melting point quaternary salt (42.3 wt% KNO_3, 39.4 wt% $CaNO_3$, 12.1 wt% $NaNO_3$, 6.1 wt% $LiNO_3$)[6]. Table 1 lists the melting temperature (T_m) for each case along with a summary of the temperature ranges over which the tests were performed (T_t) and corresponding homologous

Sandia National Laboratories is a multi-program laboratory operated and managed by
Sandia Corporation, a wholly owned subsidiary of Lockheed Martin Corporation, for the
U.S. Department of Energy's National Nuclear Security Administration under contract DE-AC04-94AL85000.

temperature ranges (T_H). Homologous temperature is defined as the temperature of a material normalized by its melting temperature using the Kelvin temperature scale (K); in this work we report T_H as a percentage value of the melting temperature ($T_H = T_t$ [K] / T_m [K]).

Salt Type and Melt Temp.	Unconfined Compressive Strength T_t [°C] / T_H [%]	Tensile Strength T_t [°C] / T_H [%]	Young's Modulus* T_t [°C] / T_H [%]	Poisson's Ratio* T_t [°C] / T_H [%]
Solar Salt [3, 4] $T_{m,A}$ = 494 K	21-127 / 60-81	24-127 / 60-81	21-127 / 60-81	21-127 / 60-81
HITEC [5] $T_{m,B}$ = 415 K	21-84 / 71-86	28-84 / 73-86	21-84 / 71-86	21-84 / 71-86
Quaternary [6] $T_{m,C}$ = 363 K	21-39 / 81-86	27-40 / 83-86	21-39 / 81-86	21-39 / 81-86

* Determined from unload/reload cycles

Table 1. Test matrix for temperature dependent mechanical testing.

Data collected in the experimental study includes force, temperature, and axial and radial displacements. Typically, these data are acquired using electronic transducers in which the electrical output is proportional to the change in the measured variable. In all cases, the constants of proportionality were determined through careful calibration using standards traceable to the National Institute for Standards and Technology.

2.1 Sample Preparation

Cylindrical samples (with diameter of approximately 5.08 cm and cut to length) were cast in a PTFE tube with silicone stopper and extracted for property testing (see Figure 1a-b). Molten salt was poured so as to fill the PTFE tube contiguously and avoid layer formation in the salt. The samples were cooled at room temperature. Cratering near the top of the samples (due to phase-dependent density change) and void formation in the salt-core interior were avoided by cross-sectioning and identifying unaffected regions of the solidified salt (Figure 1c). Solar salt has a high coefficient of thermal expansion (4.6%) and as a result, cratering of this type was most pronounced in this salt type [3, 4]. The quaternary salt had no visible cratering.

(a) (b) (c)

Figure 1. (a) Prepared salt sample, (b) heating system and fixtures, (c) void formation in Solar Salt.

The unconfined compressive strength (UCS) test was used to determine compressive strength. Unload and reload cycles performed during this test were used to obtain Young's modulus and Poisson's ratio. The indirect tensile test (also known as a Brazilian disc tension test) commonly used on rock and concrete, was employed to generate a nearly uniform tensile stress distribution normal to the compression-loaded vertical

plane to obtain tensile strength data.

Samples were cut to length using a wire saw. Unconfined compressive strength (UCS) samples were cut from near the bottom of each casting while maintaining an approximate 2/1 length-to-diameter ratio (L/D). Next, the specimens were mounted in a surface grinder where the ends of the specimens were carefully ground flat and parallel to within a tolerance of 0.0254 mm (0.001 inches). Preparation of the UCS samples followed the general outline given by ASTM Standard D4543 [7]. One sample of each salt type was turned down to a smaller diameter using a lathe. This operation was done to ensure the UCS could be obtained within the capacity of the loading frame used for elevated temperature testing. All other UCS testing was performed on as-received sample diameters.

Specimens used for tensile strength determinations were sawn from cast cylinders to produce L/D ratios of 0.5; the ends of the specimen were not ground. For indirect tension specimens (also referred to as Brazilian disc tension tests), the sides were left undressed to avoid damage that could occur in standard machining operations. Indirect tension specimens were prepared following the general outline given by ASTM Standard D3967-08 [8].

At the completion of the specimen preparation step, the density of each test specimen was calculated from the measured mass divided by the sample volume calculated from the specimen dimensions, assuming each specimen was a perfect cylinder. Each sample was labeled as follows: project (SS) – type of test (UC = unconfined compression test, BZ = Brazil) – nominal test temperature (in °C) – sample material (A = solar salt, B = HITEC, C = quaternary salt) – sample number. For example, SS-UC21-B02 indicates an unconfined compression test at room temp with HITEC salt on sample 2.

2.2 Tensile strength test method

Tensile strength was determined using ASTM D3967-08 [8]. However, this method could not be followed explicitly. An initial trial test concluded that a higher loading rate was required, above the recommended guidelines. The higher loading rate was necessary to counter sample creep at elevated temperatures so as to induce sample failure before large creep deformations occur.

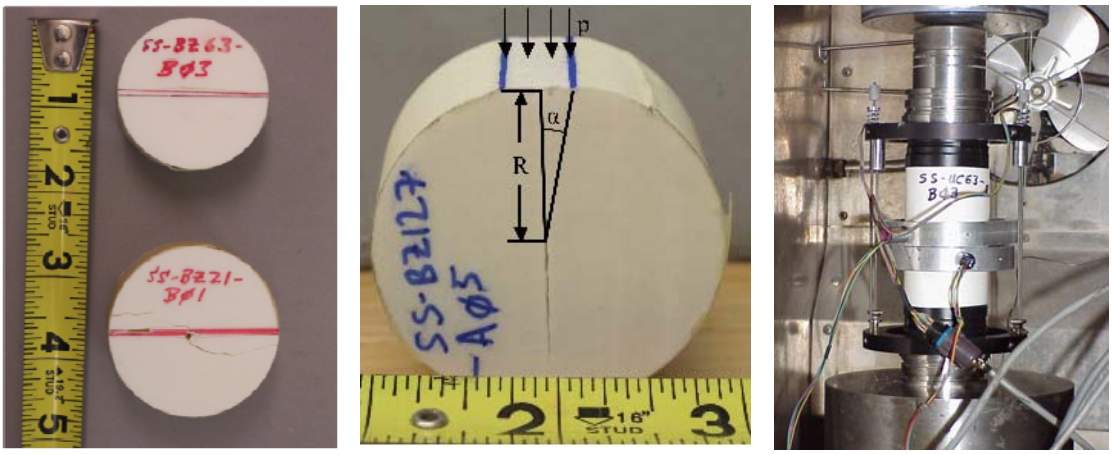

(a) (b) (c)

Figure 2. (a) Post indirect tensile strength test images of samples SS-BZ63-B03 and SS-BZ21-B01. Note the horizontal diametric crack along which the samples break when deformed. (b) Example of load distributed over an area for an elevated temperature indirect tensile test. (c) UCS test instrumented with axial and lateral displacement transducers in environmental chamber.

The splitting tensile strength test (or Brazilian test) is an indirect method for determining tensile strength because compressive stresses are applied in one direction that, in turn, induce tensile stresses in an orthogonal direction. Tensile strength can also be determined using a direct-pull, uniaxial test configuration, but such a method is more difficult to perform and more expensive when compared to the indirect method. Therefore,

tensile strengths measured in this study made use of the indirect method and thus will be referred to as indirect tensile strengths. In the splitting tensile strength test, typically a rock disk, having a L/D = 0.5, is diametrically loaded between rigid platens (with bearing strips) until failure occurs. Because of the arc shape of the disks, the loading is assumed to be along a line rather than distributed over some area. When the compressive line loading induces tensile stresses that reach the tensile strength of the material, the material fails typically by means of a vertical fracture parallel to the compressive line load (Figure 2a,b). The splitting tensile strength is calculated as,

$$\sigma_t = 2P/\pi LD \tag{1}$$

where σ_t is the splitting tensile strength [Pa], P is the maximum applied load [N], L is specimen thickness [m], and D is the specimen diameter [m].

2.3 Unconfined compressive strength test method

UCS tests were conducted by applying compressive loads to the ends of right-circular cylindrical salt specimens (L/D ≈ 2) in axial strain control until failure occurred as denoted by a drop in the axial load. The UCS is then calculated as the peak or maximum compressive force applied to the sample ends divided by the sample cross-sectional area. Electronic transducers were mounted on the test samples to measure axial and lateral sample deformations (Figure 2c illustrates a typical instrumented UCS sample and shows the axial and lateral linear variable differential transformer (LVDT) displacement transducers). Data acquired from the LVDTs together with axial stress were used to determine elastic properties such as Young's modulus and Poisson's ratio. During elevated temperature testing, samples were placed inside an environmental chamber (Figure 2c) that controlled the temperature to within ± 1 °C.

For some room-temperature tests, the axial load required to fail the samples exceeded the 22,000 lbs. capacity of the two-column reaction frame used with the environmental chamber test stand. As a result, subsequent room-temperature tests were conducted on a larger capacity (220,000 lbs.) four-column load frame. Each load frame is equipped with a load cell placed in line with the sample to measure the axial force applied to the sample ends. The first UCS test was conducted at an axial strain rate of 1×10^{-4}/sec. However, sample creep was observed during the unload/reload loops performed for elastic property determination so all subsequent tests were performed using an axial strain rate of approximately 1×10^{-3}/sec to mitigate most of the sample creep and ensure accurate determination of material properties.

3. Results and Discussion

3.1 Indirect tensile test

Table 2 (appendix) summarizes the results for all indirect tension tests. Seventeen tests were completed successfully: Seven for solar salt, six for HITEC, and four for the quaternary salt. Early in the testing series, samples were placed between cardboard loading strips. Because of the high deformation observed in the material, the cardboard loading strips were removed to aid in sample failure. Subsequent samples were taped around the circumference with two layers of masking tape. The masking tape served two purposes in that it acted as a very thin loading strip and also kept the sample intact after failure. Sample SS-BZ127-A05 did not fail as noted in Table 2 (appendix) so the tensile strength was determined from the load that was observed coincident with the greatest deformation.

Indirect tensile test temperatures for solar salt were adjusted downward from the temperatures given in the test matrix (Table 1). Large deformations were observed while testing specimen SS-BZ127-A05 at 127 °C so it was decided to test two samples at 78 °C (i.e., a homologous temperature $T_H = 0.71$). This temperature was selected because it allowed for a direct comparison of results between solar salts and HITEC at an equivalent homologous temperature (i.e., 71%). In addition, one test at 63°C ($T_H = 0.68$) was completed on solar salt to provide data at an intermediate temperature.

Many indirect tension test samples, especially those tested at elevated temperature, exhibited large deformation before failure. As a result, the curved surfaces of the test samples in contact with the loading

platens flattened such that the applied line load transitioned to a load distributed over the flattened area. Figure 2b shows an example where the load is distributed over a flattened area before failure. Distributed loads with an arc of 15° or less give similar tensile strength values as those derived from line loads and fail with similar diametral fractures provided the load is corrected to account for the contrast between line loading and distributed loading [9]. Table 2 (appendix) lists two columns for tensile strength, one in which the line load assumption is valid (i.e., no observed flattening of the samples) and one in which the line load assumption is invalid (significant flattening is observed). This latter tensile strength is defined in Table 2 (appendix) as corrected tensile strength. The flattened lengths (distance between the blue lines shown in Figure 2b) for those tests in which the line load assumption is invalid were measured post-test and are also given in Table 2 (appendix). The corrected failure load is given by [9],

$$W = 2p\alpha r \tag{2}$$

where W is the corrected load at failure [N], p is the load per unit length [N/m], α is half the angle subtended by the flattened region [rad] and r is the specimen radius [m]. Using the calculated corrected load, the corrected indirect tensile strength ($\sigma_{t,c}$) can be calculated by replacing the maximum applied load (P) in equation 1 with the corrected failure load (W, equation 2).

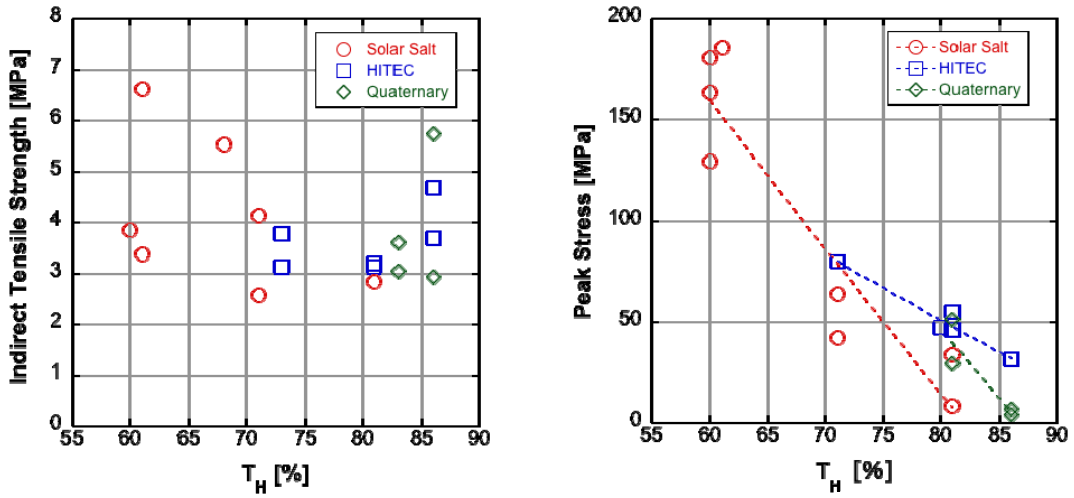

(a) (b)

Figure 3. (a) Indirect tensile strength and (b) peak stress from UCS testing vs. homologous temperature for solar salt, HITEC salt and a quaternary salt (see also Table 2 and Table 3, appendix).

Figure 3a plots indirect tensile strength versus T_H for all salt types. The variability in tensile strength at all temperatures for each salt type is large but not atypical of this type of index test measurement. For a given test temperature, the weakest sample from repeated tests is approximately 50% of the strength of the strongest sample for the same salt type, a trend also seen in natural domal salts. All salt types are much stronger than naturally occurring domal salts. A typical upper range of indirect tensile strength for domal salts is 2.07 MPa (300 psi). A strong dependence of indirect tensile strength on temperature is not observed over the temperature ranges tested for this small data set. The average indirect tensile strength for solar salt, HITEC and the quaternary salt is 4.13, 3.60, and 3.83 MPa, respectively.

3.2 Unconfined compression strength tests

The UCS tests of all three salts were determined by standard compression tests of right circular cylinders as described previously. Seventeen tests were completed: eight for solar salt, five for HITEC, and four for the quaternary salt. Table 3 (appendix) lists the peak stress observed in each test along with the density for all samples. Although peak stress is generally synonymous with UCS, there were a few tests in which UCS

could not be obtained because loading needed to be stopped before a stress drop (failure) was observed given the large sample deformations that occurred. In these cases, the peak stress was reported although this stress may be somewhat lower than the actual UCS. Typically, mechanical properties such as UCS and Young's modulus are correlated with physical properties such as density. However, in this study, temperature is varied and is the dominant factor affecting changes in both UCS and elastic properties and given the limited number of tests performed, the focus of the subsequent analysis is on temperature effects.

Figure 3b plots peak stress versus homologous temperature (test temperature) for all UCS samples. Linear fits using a least squares regression are given for each salt type comparing UCS (or peak stress) to homologous temperature. For all salt types, UCS decreases as homologous temperature increases. Scatter in the data is observed and is expected for this type of index test and material. Although an effort was made to avoid sections of salt with high void content (Figure 1c), some of the scatter in strength could be attributed to small voids in individual samples. Variations in void concentration will impact sample density. However, there does not appear to be an obvious trend between density and UCS in these results. If a correlation does exist for density and other mechanical properties, it is likely overshadowed by temperature variations and the relative small range of densities observed for the test specimens.

3.3 Young's modulus and Poisson's ratio

Young's modulus (E) and Poisson's ratio (ν) were determined from true axial stress versus true strain data using least squares linear regression. Young's modulus is defined as,

$$E = \Delta\sigma_a / \Delta\varepsilon_a \tag{3}$$

where $\Delta\sigma_a$ is the change in true axial stress and $\Delta\varepsilon_a$ is the corresponding change in true axial strain. Poisson's ratio is defined as,

$$\nu = E \Big/ \left(\Delta\sigma_a / \Delta\varepsilon_l\right) \tag{4}$$

where $\Delta\varepsilon_l$ is the change in true lateral strain corresponding to the change in true axial stress. An example stress versus strain plot is shown in Figure 4a. Figure 4b shows a zoomed in region of Figure 4a and illustrates the linear regions used in calculating E and ν in the unload/reload cycles.

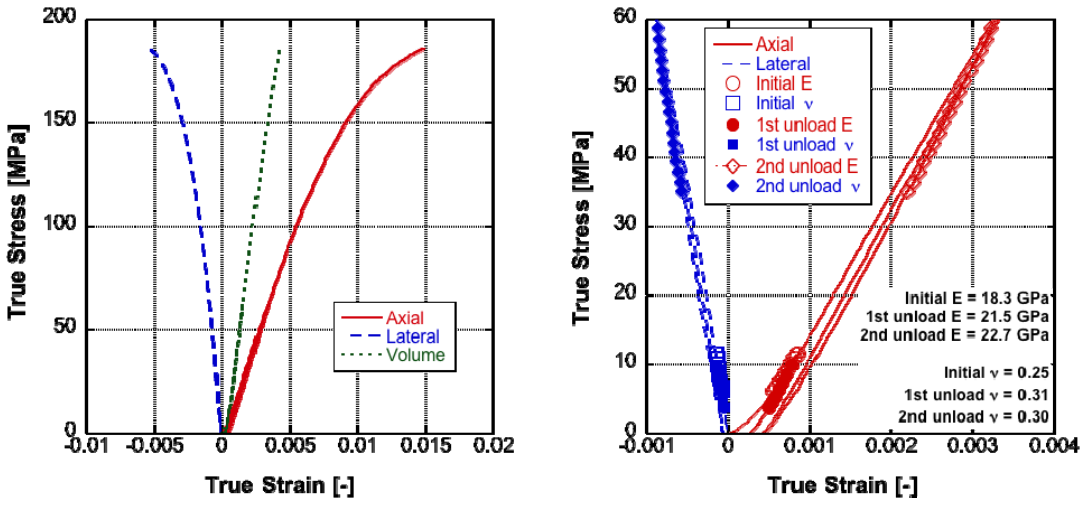

Figure 4. True stress versus true strain for sample SS-UC27-A08 (a) for multiple unload/reload cycles and a (b) zoomed in view including linear regions sampled for E and ν (variance in E and ν values provided in the inset for multiple runs).

Table 4 (appendix) shows all calculated E and ν values. The column labeled 'stress at unload' is the highest

axial stress in the interval where E and ν were determined. The stress at unload is only given for elastic properties calculated from unload/reload cycles. A few of the ν values are above 0.5. For all these cases, the sample had reached dilation (the stress at which volumetric strain attains its most positive value, sample compaction) and then trends toward smaller values with additional loading. When salt dilates, micro-cracks form and the material begins to rapidly expand in the radial direction leading to negative volumetric strains.

Figure 5 illustrates the relationship of E and ν with homologous temperature for all salt types. Least squares linear regression fits are presented for the E and ν trends with temperature. All elastic properties are plotted including initial E and ν values as well as those calculated from the unload/reload cycles. All three salts exhibit a decrease in E with increasing temperature likely due to material softening with increasing temperature. Poisson's ratio tends to increase with increasing temperature. For the quaternary salt, a possible outlier in the data has been excluded from the trend line fit. The possible outlier is plotted for completeness.

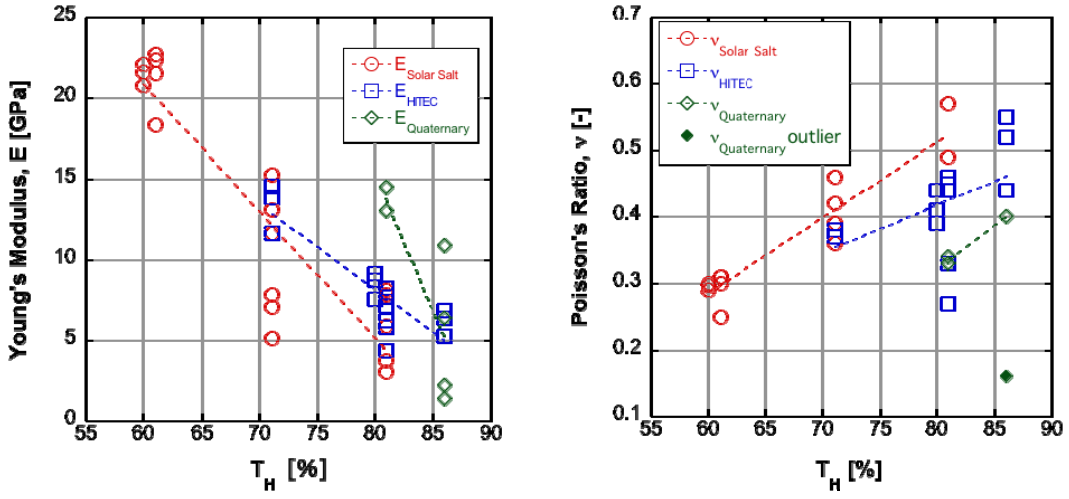

Figure 5. (a) Young's modulus and (b) Poisson's ratio as a function of homologous temperature (see also data in Table 4, appendix.).

4. Conclusion

Three salt compositions for potential use in concentrating solar power were tested to determine their mechanical properties as a function of temperature. The mechanical properties determined were unconfined compressive strength, Young's modulus, Poisson's ratio, and indirect tensile strength. Seventeen uniaxial compression and indirect tension tests were completed. It was found that as test temperature increases, unconfined compressive strength and Young's modulus decrease for all salt types. Poisson's ratio tends to increase with increasing temperature. The variability in measured indirect tensile strength is large, but not atypical for this index test. The average tensile strength for all salt types tested is substantially higher than the upper range of tensile strengths for naturally occurring rock salts.

References

[1] Kearney D., Herrmann U., Nava P., Kelly B., Mahoney R., Pacheco J., Cable R., Potrovitza N., Blake D., and Price H., "Assessment of a molten salt heat transfer fluid in a parabolic trough solar field," *Journal of Solar Energy Engineering*, 125 (2003) 170-176.

[2] Kolb G. J., Ho C., Iverson B. D., Moss T. A., and Siegel N. P., "Freeze-thaw tests of trough receivers employing a molten salt working fluid," ASME Energy Sustainability (2010) Phoenix, AZ, USA, May 17-22, 2010.
[3] Pacheco J. E., Ralph M. E., Chavez J. M., Dunkin S. R., Rush E. E., Ghanbari C. M., and Matthews M. W., "Results of molten salt panel and component experiments for solar central receivers: cold fill, freeze/thaw, thermal cycling and shock, and instrumentation tests," Sandia National Laboratories (1994) SAND94-2525.
[4] Bradshaw R. W. and Carling R. W., "A review of the chemical and physical properties of molten alkali nitrate salts and their effects on materials used for solar central receivers," Sandia National Laboratories (1987) SAND87-8005.
[5] Coastal Chemical Company, HITEC Heat Transfer Salt, retrieved April 19, 2010, from http://www.coastalchem.com/process-literature-files.html
[6] Bradshaw R. W., Cordaro J. G., and Siegel N. P., "Molten nitrate salt development for thermal energy storage in parabolic trough solar power systems," ASME Energy Sustainability (2009) San Francisco, CA, July 19-23, 2009.
[7] ASTM D4543, 1995, *Standard practice for preparing rock core specimens and determining dimensional and shape tolerances*, American Society for Testing and Materials, (1995).
[8] ASTM D3976-08, 2008, *Standard test method for splitting tensile strength of intact rock core specimens*, American Society for Testing and Materials, (2008).
[9] Jaeger J. C. and Cook N. G. W. (1979) *Fundamentals of Rock Mechanics*, Third ed., Chapman and Hall, London.

Appendix

Sample	Test Temp. T_t [°C]	Homologous Temp. T_H [%]	Density [g/cc]	Indirect Tensile Strength [MPa]	Flattened Length [mm]	Corrected Tensile Strength*** [MPa]
*SS-BZ27-A01	27	61	2.16	N/A	0	N/A
*SS-BZ27-A02	27	61	2.17	6.62	0	6.62
SS-BZ27-A04	27	61	-	3.37	0	3.37
SS-BZ24-A08	24	60	2.13	3.85	0	3.85
SS-BZ63-A03	63	68	-	5.54	0	5.54
SS-BZ78-A06	78	71	-	2.64	7.3	2.57
SS-BZ78-A07	78	71	2.17	4.18	4.9	4.13
**SS-BZ127-A05	127	81	2.15	3.05	11.9	2.84
SS-BZ28-B01	28	73	2.11	3.12	0	3.12
SS-BZ29-B02	29	73	2.11	3.77	0	3.77
SS-BZ63-B03	63	81	2.09	3.24	4.2	3.20
SS-BZ63-B05	63	81	2.11	3.16	3.8	3.13
SS-BZ84-B04	84	86	2.08	4.86	7.6	4.68
SS-BZ84-B06	84	86	2.11	3.79	6.9	3.68
*SS-BZ27-C01	27	83	2.15	3.59	0	3.59
SS-BZ27-C03	27	83	-	3.05	0	3.05
SS-BZ39-C02	40	86	2.18	5.74	0	5.74
SS-BZ39-C04	39	86	2.19	2.94	0	2.94

N/A = load control of sample lost during test
**Sample did not break
*Cardboard loading strips
***Jaeger and Cook, Figure 6.11.1c [9]

Table 2. Indirect tension test results.

Sample	Length [cm]	Diameter [cm]	Weight [g]	Density [g/cc]	Test Temp. T_t [°C]	Homologous Temp. T_H [%]	Peak Stress [MPa]
*SS-UC21-A05	9.26	4.36	299.8	2.17	21	60	129.62
*SS-UC21-A06	9.59	4.36	310.3	2.17	21	60	163.16
SS-UC23-A07	9.69	4.37	314.8	2.17	23	60	180.32
SS-UC27-A08	8.96	4.35	289.5	2.18	27	61	185.75
SS-UC78-A02	9.13	4.38	294.7	2.15	78	71	63.65
SS-UC78-A04	8.83	3.97	235.0	2.15	78	71	42.22
SS-UC127-A01	8.88	4.37	288.6	2.17	127	81	33.93
SS-UC127-A03	9.18	4.35	297.6	2.18	127	81	8.28
SS-UC21-B02	10.54	4.95	423.7	2.09	21	71	79.92
SS-UC57-B03	10.40	4.98	427.8	2.11	57	80	47.48
SS-UC63-B04	8.96	4.37	284.3	2.12	63	81	54.85
SS-UC63-B05	8.94	4.04	242.4	2.11	63	81	46.08
SS-UC84-B06	9.24	4.36	294.2	2.13	84	86	31.87
SS-UC21-C01	10.57	5.00	N/A	N/A	21	81	51.11
*SS-UC21-C04	8.95	4.21	276.6	2.22	21	81	29.28
SS-UC39-C02	10.42	5.01	449.7	2.19	39	86	3.70
SS-UC39-C03	10.34	5.04	448.7	2.18	39	86	6.68

N/A = Weight and density not determined pre-test
*Peak stress defined in terms of engineering stress; all others in terms of true stress

Table 3. UCS test results: density and peak stress.

Sample	Test Temp. T_t [°C]	Homologous Temp. T_H [%]	Young's Modulus, E [GPa]	Stress at unload* [MPa]	Poisson's Ratio, ν [-]
SS-UC21-A05	21	60	N/A		N/A
SS-UC21-A06	21	60	N/A		N/A
SS-UC23-A07	23	60	20.75		0.29
SS-UC23-A07	23	60	21.58	17.00	0.30
SS-UC23-A07	23	60	22.06	47.86	0.30
SS-UC23-A07	27	61	22.34	131.08	0.31
SS-UC27-A08	27	61	18.34		0.25
SS-UC27-A08	27	61	21.51	9.78	0.31
SS-UC27-A08	27	61	22.68	55.52	0.30
SS-UC78-A02	78	71	11.65		0.36
SS-UC78-A02	78	71	15.31	8.63	0.36
SS-UC78-A02	78	71	13.10	27.84	0.42
SS-UC78-A04	78	71	5.12		0.39
SS-UC78-A04	78	71	7.10	6.61	0.46
SS-UC78-A04	78	71	7.86	11.62	0.46
SS-UC127-A01	127	81	5.93		N/A
SS-UC127-A01	127	81	8.14	5.25	N/A
SS-UC127-A01	127	81	7.86	10.58	N/A
SS-UC127-A03	127	81	3.79		0.49
SS-UC127-A03	127	81	3.08	2.56	**0.57
SS-UC21-B02	21	71	11.65		0.38
SS-UC21-B02	21	71	14.62	25.99	0.37
SS-UC21-B02	21	71	13.86	40.69	0.38
SS-UC57-B03	57	80	7.58		0.41
SS-UC57-B03	57	80	9.17	4.12	0.39
SS-UC57-B03	57	80	8.76	9.11	0.44
SS-UC63-B04	63	81	5.86		0.46
SS-UC63-B04	63	81	7.72	6.72	0.45
SS-UC63-B04	63	81	7.17	11.34	0.44
SS-UC63-B05	63	81	4.36		0.27
SS-UC63-B05	63	81	6.23	2.34	0.33
SS-UC63-B05	63	81	8.27	10.85	0.44
SS-UC84-B06	84	86	5.25		0.44
SS-UC84-B06	84	86	6.86	4.35	**0.52
SS-UC84-B06	84	86	6.43	7.65	**0.55
SS-UC21-C01	21	81	13.03		0.33
SS-UC21-C01	21	81	14.55	21.24	0.34
SS-UC21-C04	21	81	N/A		N/A
SS-UC39-C02	39	86	1.38		N/A
SS-UC39-C02	39	86	6.37	1.65	N/A
SS-UC39-C03	39	86	2.21		0.16
SS-UC39-C03	39	86	10.89	2.36	0.40

N/A = Data not recorded during test
*Initial elastic properties do not list the axial stress where the modulus was calculated
**Poisson's ratio over 0.5 occured during sample dilation

Table 4. UCS test results: Young's modulus and Poisson's ratio.